Journal of Biomechanics 122 (2021) 110413

Contents lists available at ScienceDirect

Journal of Biomechanics

journal homepage: www.elsevier.com/locate/jbiomech
www.JBiomech.com

The effects of a simple optical clearing protocol on the mechanics of collagenous soft tissue

William D. Meador [a], Jennifer Zhou [a], Marcin Malinowski [b,c], Tomasz Jazwiec [b,d], Sarah Calve [e], Tomasz A. Timek [b], Manuel K. Rausch [a,f,g,*]

[a] Department of Biomedical Engineering, University of Texas at Austin, Austin, TX, United States
[b] Division of Cardiothoracic Surgery, Spectrum Health, Grand Rapids, MI, United States
[c] Department of Cardiac Surgery, Medical University of Silesia, School of Medicine in Katowice, Katowice, Poland
[d] Department of Cardiac, Vascular and Endovascular Surgery and Transplantology, Medical University of Silesia in Katowice, Silesian Centre for Heart Diseases, Zabrze, Poland
[e] Department of Mechanical Engineering, University of Colorado – Boulder, Boulder, CO, United States
[f] Department of Aerospace Engineering & Engineering Mechanics, University of Texas at Austin, Austin, TX, United States
[g] Oden Institute for Computational Engineering and Sciences, University of Texas at Austin, Austin, TX, United States

ARTICLE INFO

Article history:
Accepted 20 March 2021

Keywords:
Two-photon
Microscopy
Multi-scale
Biaxial
Leaflet

ABSTRACT

Optical clearing of biological tissues improves imaging depth for light transmission imaging modalities such as two-photon microscopy. In studies that investigate the interplay between microstructure and tissue-level mechanics, mechanical testing of cleared tissue may be useful. However, the effects of optical clearing on soft tissue mechanics have not been investigated. Thus, we set out to quantify the effects of a simple and effective optical clearing protocol on the mechanics of soft collagenous tissues using ovine mitral valve anterior leaflets as a model system. First, we demonstrate the effectiveness of an isotonic glycerol-DMSO optical clearing protocol in two-photon microscopy. Second, we evaluate the mechanical effects of optical clearing on leaflets under equibiaxial tension in a dependent study design. Lastly, we quantify the shrinkage strain while traction-free and the contractile forces while constrained during clearing. We found the optical clearing protocol to improve two-photon imaging depth from ~100 μm to ~500–800 μm, enabling full-thickness visualization of second-harmonic generation, autofluorescent, and fluorophore-tagged structures. Under equibiaxial tension, cleared tissues exhibited reduced circumferential ($p < 0.001$) and radial ($p = 0.009$) transition stretches (i.e. stretch where collagen is recruited), and reduced radial stiffness ($p = 0.031$). Finally, during clearing we observed ~10–15% circumferential and radial compressive strains, and when constrained, ~2 mN of circumferential and radial traction forces. In summary, we suggest the use of this optical clearing agent with mechanical testing be done with care, as it appears to alter the tissue's stress-free configuration and stiffness, likely due to tissue dehydration.

1. Introduction

Modern imaging modalities such as confocal microscopy, optical coherence tomography, and multi-photon microscopy provide unprecedented insight into the microstructure of collagenous soft tissues (Fujimoto, 2003; Goth et al., 2016; Helmchen and Denk, 2005). For example, two-photon (2P) microscopy allows quantifying microstructural information about soft collagenous tissues to significant depth without the invasive effects of fixation as is necessary with classic histology/immunohistochemistry. The power of 2P microscopy is further enhanced through the autofluorescent and second-harmonic generation (SHG) properties of elastin and collagen, respectively, that can now be visualized without need for fluorescent agents (Cox and Kable, 2006; Deyl et al., 1980; Schenke-Layland, 2008). Nevertheless, fluorescent labelling can further enrich 2P target visualization (So et al., 2000). To this end, we have recently developed an imaging protocol to simultaneously visualize tissue microstructure (i.e., elastin, collagen, and cell nuclei) using a 2P microscope without tissue fixation.

With this imaging protocol, we recently sought to perform mechanical tests under a 2P microscope to study the multi-scalar interplay between microstructure and tissue-level mechanics. As most soft tissues are layered, heterogeneous structures, through-

* Corresponding author at: 2617 Wichita Street, Austin, TX 78712, United States.
E-mail address: manuel.rausch@utexas.edu (M.K. Rausch).
URL: http://www.manuelrausch.com (M.K. Rausch).

https://doi.org/10.1016/j.jbiomech.2021.110413
0021-9290/

depth information is critically important to our understanding of this interplay (Chen and Kassab, 2016; Meador et al., 2020a, 2020b). However, we found 2P microscopy depth penetration to be insufficient for full-depth image acquisition, limited to only about 100 μm in murine skin and ovine heart valve leaflets (Meador et al., 2020a, 2020b). A solution to this limitation is to use one of numerous optical clearing protocols ranging in complexity to improve light penetration of tissues (Costantini et al., 2019; Tuchin, 2005; Zhu et al., 2013). However, we found no literature reports on whether optical clearing inadvertently changes the mechanical properties of tissues. Thus, the objective of this short communication was to investigate the effect of a simple, but effective, optical clearing protocol on the mechanics of soft collagenous tissues.

2. Methods

2.1. Tissue samples and storage

We isolated anterior mitral valve leaflets from healthy male Dorset sheep, 51 ± 8 kg aged 5–6 months, and stored them in a cryogenic solution (9:1 DMEM:DMSO) with protease inhibitor under a freeze rate of 1 °C/min. Before testing, we rapidly thawed the tissue to room temperature. For all tests, we isolated a 7×7 mm square belly region sample, aligned to the circumferential and radial directions.

2.2. Optical clearing

Our optical clearing solution (OCS) was informed by a previously reported solution of 50:30% glycerol:dimethyl sulfoxide (DMSO) (Xu and Wang, 2004). To reduce the likelihood of volumetric changes, we addended this OCS with 20% 5×PBS to match standard tissue tonicity. Furthermore, we physically enhanced OCS permeation via sonication and 37 °C heating (Deng et al., 2011; Xu et al., 2009). We cleared all tissues for 30 min.

2.3. Two-photon microscopy protocol

We first counterstained cell nuclei (Thermo Fisher Scientific, Hoechst 33342, Waltham, MA, US) for 20 min. With a 2P microscope (Bruker, Ultima IV, Billerica, MA, US) and 20× water immersion objective (Olympus, XLUMPLFLN, Center Valley, PA, US), we imaged a centrally located 500 × 500 μm region at 10 μm z-steps twice: once before optical clearing, and again, after clearing. Using excitation wavelengths, λ_{exc}, we epicollected the backscattered signal via photomultiplier tube (PMT) filters. Specifically, for each imaging set we collected collagen signal via SHG (λ_{exc} = 900 nm, λ_{PMT} = 460 ± 25 nm), nuclei signal via fluorophore (λ_{exc} = 800 nm, λ_{PMT} = 460 ± 25 nm), and elastin signal via autofluorescence (λ_{exc} = 900 nm, λ_{PMT} = 525 ± 25 nm). We verified full thickness acquisition via foil-lined slide visualization.

2.4. Biaxial testing protocol

On isolated tissue squares, we applied fiduciary markers in a square arrangement (3×3mm). Afterwards, we photographed the tissue on a calibrated grid while in a stress-free configuration (i.e., floating on PBS). On n = 7 samples, we performed the same mechanical testing protocol twice (Biotester, Cellscale, Waterloo, ON, Canada) without dismounting the tissue: First, in 37 °C 1×PBS, after which we replaced the PBS with our OCS (without sonication), and performed the second mechanical test 30 min later in 37 °C OCS. Between tests we did not zero load cells (1.5 N capacity, ± 1.5 mN) and tests began from identical motor positions. During both tests, we performed 10 preconditioning cycles equibiaxially to 500 mN, preloaded 10 mN to remove slack, and tested 2 final equibiaxial cycles to 500 mN. We recorded the final downstroke rake-to-rake distances, radial and circumferential forces, and fiduciary marker images at 5 Hz. Using the marker positions, we calculated the deformation gradient tensor, $\boldsymbol{F}$, from a stress-free reference configuration. We acquired in-test stretches from the right Cauchy-Green deformation tensor, $\boldsymbol{C}$, via $\boldsymbol{C} = \boldsymbol{F}^T\boldsymbol{F}$. We calculated the membrane tension as the measured force divided by the sample width. To characterize the resulting nonlinear tension-stretch curves, we identified four metrics: toe stiffness (i.e., lower region slope), calf stiffness (i.e., upper region slope), transition stretch (i.e., stretch data point nearest intersection of lower and upper region slope), and degree of anisotropy (i.e., circumferential to radial stretch ratio at 50 N/m). We also repeated this entire protocol for a negative control (n = 3), where the tissue was tested twice in 37 °C 1×PBS, separated by a 30 min interval.

2.5. Clearing mechanics

On a separate set of tissue samples (n = 3, per condition), we applied a 5 × 5 mm ink stamp to each sample. We measured circumferential and radial strain after 30 min of clearing under two conditions: (i) while traction-free (i.e., floating in OCS), and (ii) while constrained (i.e., mounted on biaxial device, without preload). After 30 min, we photographed all samples while floating on OCS on a calibrated grid every 5 min for 30 more minutes. Tissue remained traction-free in OCS between pictures. We determined $\boldsymbol{F}$and $\boldsymbol{C}$ from the stamp dimensions for each image, as before. We calculated Green-Lagrange Strain tensor, $\boldsymbol{E}$, via $\boldsymbol{E} = 1/2(\boldsymbol{C} - \boldsymbol{I})$,where $\boldsymbol{I}$ is the 2nd order identity tensor. During constrained clearing, we also measured radial and circumferential forces for 30 min.

2.6. Statistics

For data comparisons, we performed Shapiro-Wilk tests to probe data normality. If normality assumptions were upheld, we performed paired Student's t-tests. Otherwise, we performed Wilcoxon Signed-Rank tests. We define significance as $p < 0.05$.

3. Results

3.1. Optical clearing enables full thickness 2P microscopy for mitral valve leaflets

The optical clearing protocol used in this study improved the optical clarity of mitral valve anterior leaflets (Fig. 1A). During 2P microscopy of uncleared samples, image acquisition depth was limited to around 100 μm (Fig. 1B-C). However, after optical clearing, image acquisition depth was improved to over 600 μm and enabled full-thickness acquisition of SHG, autofluorescent, and fluorophore labelled structures. Overall, this optical clearing protocol improved 2P microscopy imaging depth and enabled full-thickness acquisition for mitral valve anterior leaflets (~500–800 μm).

3.2. Optical clearing reduces transition stretches and reduces radial stiffness

To evaluate the effects of optical clearing on mechanics, we equibiaxially tested n = 7 square samples from mitral valve anterior leaflets under a dependent experimental setup (i.e., repeat testing of same samples before and after clearing, without dismounting). We found that all samples, before and after clearing, exhibited classic non-linear J-shaped loading behavior, as expected

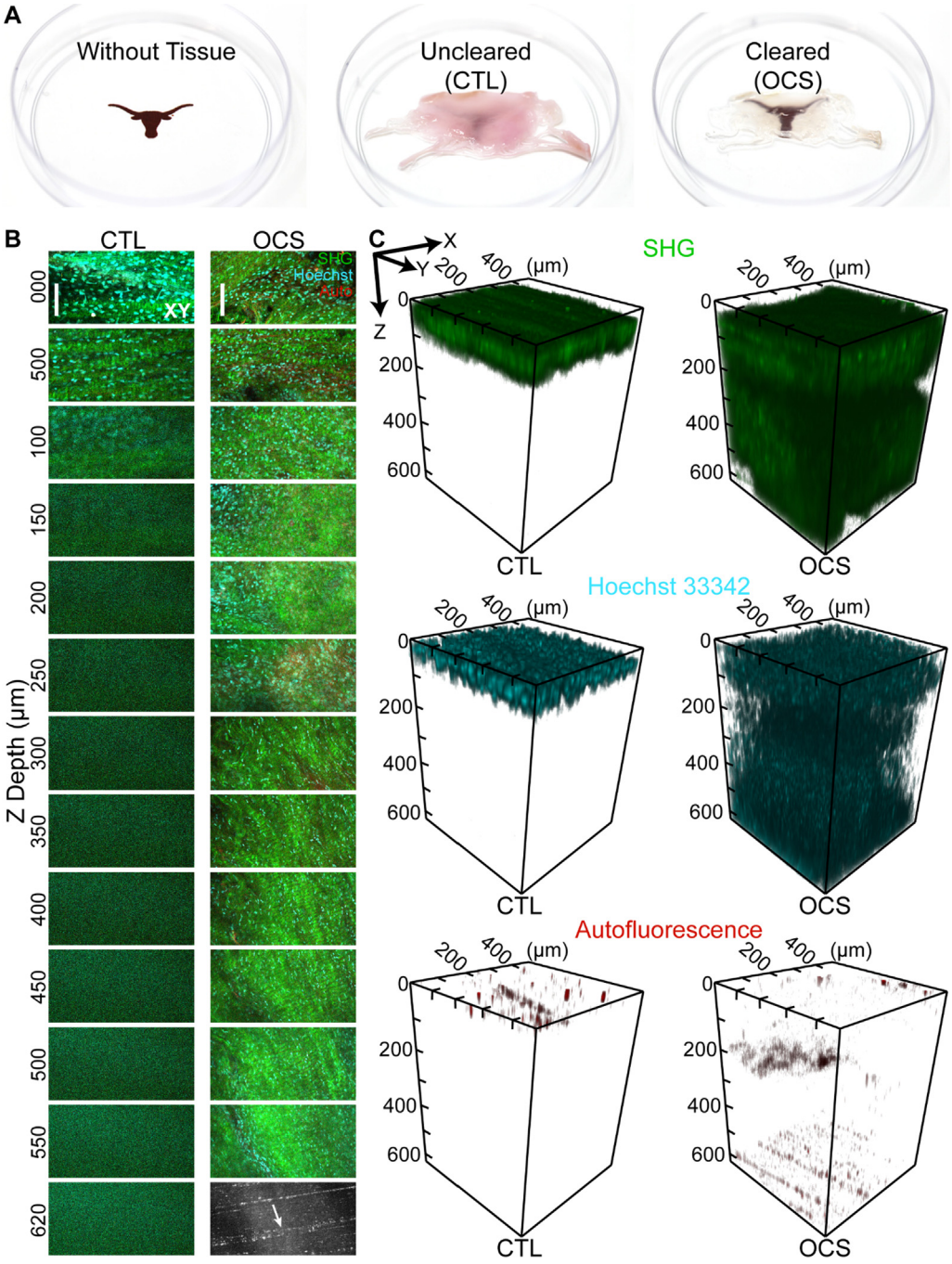

Fig. 1. Effectiveness of simple clearing protocol used in this study. **(A)** A mitral valve anterior leaflet prior to clearing (middle, control, CTL) and after optical clearing solution (OCS) protocol (right) with a background graphic (left) to demonstrate optical clarity. **(B)** Two-photon image composites of collagen via second harmonic generation (SHG, green), cell nuclei via Hoechst 33342 fluorescence (cyan), and elastin via autofluorescence (red). Images are organized as depth z-stacks for the same sample before clearing (CTL, left) and after clearing (OCS, right), with acquisition depth listed in rows. In the CTL sample, clear images of the target constituents fade beyond 100 μm depths, while in the same sample after clearing, we acquired clear images throughout the full tissue thickness, demonstrated by visualization of the aluminum foil-lined microscope slide (white arrow, black and white image). Scale bar = 100 μm **(C)** 3D visualization of two-photon acquired z-stacks between CTL and OCS treated tissues for SHG (green), Hoechst 33342 (cyan), and autofluorescence (red). (For interpretation of the references to colour in this figure legend, the reader is referred to the web version of this article.)

for collagenous tissues (Eilaghi et al., 2010; Sacks, 2000) (Fig. 2A). Qualitatively, we observed the cleared tissue curves to shift left (i.e., become less compliant) in both circumferential and radial directions relative to the uncleared curves. To quantify our qualitative observations, we measured four metrics for the non-linear curves: toe region stiffness, calf region stiffness, transition stretch, and degree of anisotropy (Fig. 2B). We found that circumferential and radial toe region stiffness remained similar before and after clearing (Fig. 2C). However, we did find a significant reduction in radial calf region stiffness in cleared tissues ($p = 0.031$) (Fig. 2D). Furthermore, there were significant decreases in both circumferential and radial transition stretches for cleared samples ($p = 0.0003$ and $p = 0.0087$, respectively), confirming our qualitative observation (Fig. 2E). Despite these shifts in transition stretches, we did not find differences in anisotropy between cleared and uncleared samples (Fig. 2F). To verify that these changes were resultant from the optical clearing solution rather than repeated testing, we performed $n = 3$ negative control tests in 37 °C 1×PBS over the same

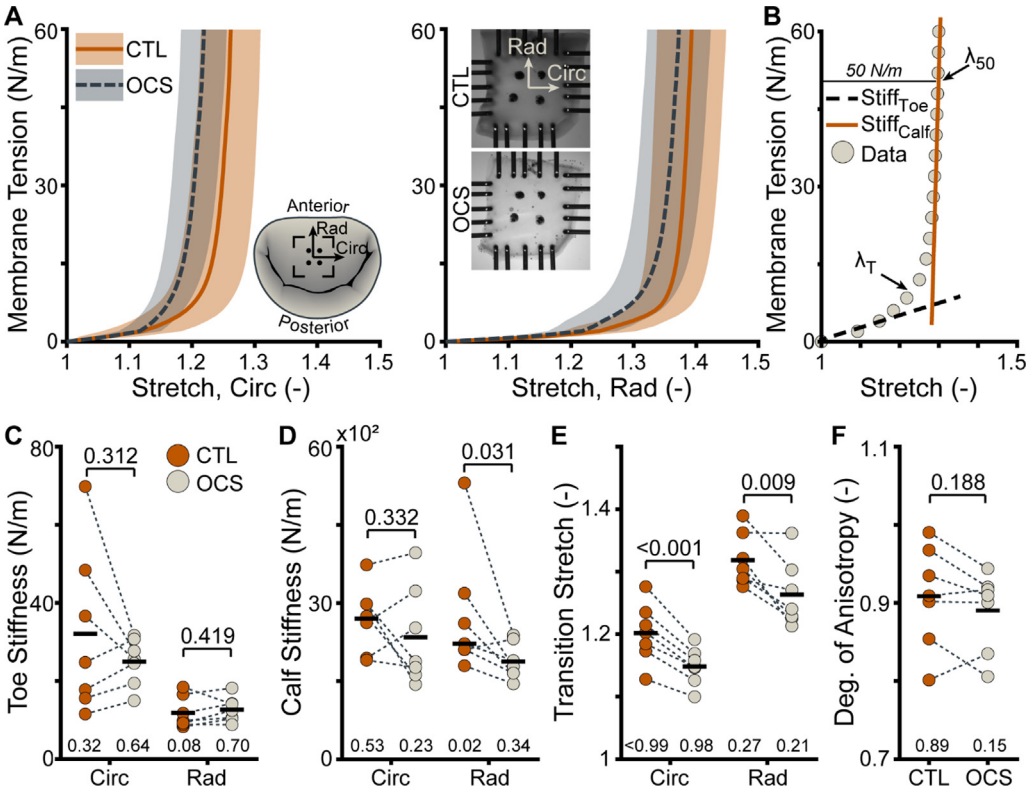

Fig. 2. Optical clearing alters collagenous soft tissue equibiaxial mechanics. **(A)** Equibiaxial membrane tension-stretch curves (lines) with standard deviation (shaded) for uncleared (CTL, orange) and cleared (OCS, gray) samples in circumferential (Circ, left) and radial (Rad, right) directions. Inset on the left is a mitral valve graphic with location of biaxial sample. Insets on the right are two images of a CTL and OCS sample mounted for biaxial testing. **(B)** Diagram demonstrating the mechanical metrics quantified in **(C-F).** In brief, we calculated toe region stiffness (i.e., lower region), calf region stiffness (i.e., upper region near 50 N/m), transition stretch (λ_T, i.e., closest data point to intersection of toe and calf region stiffness projections), and degree of anisotropy (i.e., circumferential to radial ratio of stretch at 50 N/m, λ_{50}) **(C-F)** Mechanical metrics to be compared before and after clearing: **(C)** toe region stiffness, **(D)** calf region stiffness, **(E)** transition stretch, and **(F)** degree of anisotropy. Dotted lines connect matched samples before and after clearing, i.e., CTL (orange) and OCS (gray). Values below data represent p-value of Shapiro-Wilk's normality test. Values above data are p-values from paired Student's *t*-test or Wilcoxon Signed-Rank test. Black bars represent data mean, if normal, or median, if non-normal. (For interpretation of the references to colour in this figure legend, the reader is referred to the web version of this article.)

30 min time interval. As expected, we found no changes between test groups in the negative control setup (Supplemental Figure S1). Overall, we observed reduced transition stretches and reduced radial stiffness due to optical clearing.

3.3. Optical clearing results in tissue shrinkage and produces detectable forces in tissue

Because we observed tissue shrinkage during the experiments for Fig. 1A, we also set out to quantify this effect. We found that after 30 min of clearing, both traction free (i.e., floating) and traction bound (i.e., mounted biaxially) samples (n = 3, per condition) exhibited similar strain reductions to one another once removed from their relative constraints (Fig. 3A). We observed slightly less deformation in the circumferential direction (~-10%) compared to radial direction (~-15%). Shrinkage was stable during the strain measurements up to 60 min implying that the tissue had equilibrated. In those samples that were constrained we also measured produced forces and observed approximately 2 mN of force on average for the circumferential and radial directions (Fig. 3B). Overall, we observed and quantified tissue shrinking due to optical clearing, which also produced measurable traction forces when samples were constrained.Fig. 3

4. Discussion

Our work was motivated by our interest in performing mechanical testing under 2P microscopy to study the multi-scalar interplay between through-depth microstructure and tissue-level mechanics. We have previously demonstrated the effectiveness of optical clearing in obtaining through-thickness information (Meador et al., 2020a). However, before this study, it was unknown how clearing affects tissue mechanics. Therefore, we set out to quantify the mechanical differences between cleared and uncleared tissue using mitral valve anterior leaflets as a model system.

While it was not the main focus of our work to study optical clearing, we showed here that a simple, fast protocol with few steps and inexpensive reagents can be a very effective clearing agent. Specifically, we found that 2P microscopy, which we have previously found to be limited to 100 μm depth in soft collagenous tissues (Meador et al., 2020b), was able to penetrate our tissues to full thickness (~500–800 μm) with the aid of this clearing protocol. Mechanistically, our simple immersion optical clearing protocol likely functions through three synergistic mechanisms: i) tissue dehydration, ii) refractive index matching between the clearing agent and structural protein matrix, and iii) dissociation of the structural protein matrix (e.g., collagen) (Richardson and Lichtman, 2015; Rylander et al., 2006; Tuchin, 1997; Yeh et al., 2003).

Using equibiaxial tension as a physiologically relevant loading mode, we observed several significant differences between the mechanical behaviors of uncleared and cleared tissues. Clearing the tissue reduced the stretch at which collagen fiber recruitment begins (i.e., transition stretch) (Liao et al., 2007; Stella et al., 2007), caused shrinkage when traction-free, and generated tensile forces when constrained. These findings suggest that optical clearing

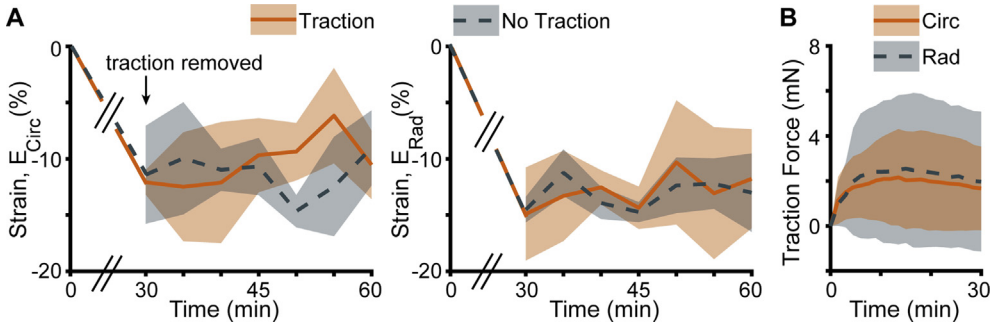

Fig. 3. Optically cleared tissues shrink and apply detectable traction forces. **(A)** Samples were optically cleared for 30 min under constrained (orange) and traction-free (gray) conditions. After 30 min, constrained samples were unloaded (arrow). In both groups, we subsequently measured circumferential (left) and radial (right) Green-Lagrange strains, E, for another 30 min. Lines represent the mean while shaded regions indicate standard deviation. **(B)** Those samples that were constrained applied circumferential (orange) and radial (gray) tensile forces during the initial 30 min of optical clearing. (For interpretation of the references to colour in this figure legend, the reader is referred to the web version of this article.)

alters the stress-free configuration of collagenous soft tissues, likely via configurational changes of structural constituents (i.e., collagen). Specifically, the clearing agent's dehydration of the tissue can produce conformational changes of collagen, resulting in molecule shortening and generation of tensile stresses (Masic et al., 2015), consistent with our observations. Interestingly, we also observed a reduction in radial calf region stiffness, perhaps due to another proposed mechanism of optical clearing agents – dissociation of the structural protein matrix (Yeh et al., 2003). As mitral valve leaflets are strongly anisotropic materials due to mostly circumferentially aligned collagen-dense fibrosa (Rausch et al., 2011; Sacks et al., 2009), this finding may suggest differential dissociation of the anisotropic protein matrix. As optical clearing has been shown to be reversible (Neu et al., 2015), similar tests on the reversibility of clearing on mechanics could answer these questions. Identification of the exact mechanisms underlying the mechanical effects of optical clearing exceeds the scope of this short communication. However, future studies, in addition to exploring the effect of other protocols, may conduct more detailed experiments to reveal this interesting interplay between optical properties and mechanics.

In conclusion, we demonstrated the effectiveness of a simple, inexpensive, and fast optical clearing protocol in improving 2P penetration depth of a soft collagenous tissue. Furthermore, we showed that this protocol altered the mechanics of tissue, likely due to collagen-driven changes to the tissue's stress-free configuration. Our data suggests that mechanical tests after optical clearing, at least with the current protocol, should be interpreted with care.

Declaration of Competing Interest

The authors declare that they have no known competing financial interests or personal relationships that could have appeared to influence the work reported in this paper.

Acknowledgements

Research reported in this publication was supported by the National Heart, Lung, And Blood Institute of the National Institutes of Health under Award Number F31HL145976 (WDM), the American Heart Association for their support under Award Number 18CDA34120028 (MKR). The content is solely the responsibility of the authors and does not necessarily represent the official views of the National Institutes of Health or the American Heart Association.

Appendix A. Supplementary material

Supplementary data to this article can be found online at https://doi.org/10.1016/j.jbiomech.2021.110413.

References

Chen, H., Kassab, G.S., 2016. Microstructure-based biomechanics of coronary arteries in health and disease. J. Biomech. 49, 2548–2559. https://doi.org/10.1016/j.jbiomech.2016.03.023.
Costantini, I., Cicchi, R., Silvestri, L., Vanzi, F., Pavone, F.S., 2019. In-vivo and ex-vivo optical clearing methods for biological tissues: review. Biomed. Opt. Express 10, 5251. https://doi.org/10.1364/BOE.10.005251.
Cox, G., Kable, E., 2006. Second-harmonic imaging of collagen. In: Methods in Molecular Biology (Clifton, N.J.). Humana Press, pp. 15–35. https://doi.org/10.1007/978-1-59259-993-6_2.
Deng, Z., Liu, C., Tao, W., Zhu, D., 2011. Improvement of skin optical clearing efficacy by topical treatment of glycerol at different temperatures. J. Phys. Conf. Ser. 277,. https://doi.org/10.1088/1742-6596/277/1/012007 012007.
Deyl, Z., Macek, K., Adam, M., Vancikova, 1980. Studies on the chemical nature of elastin fluorescence. Biochim. Biophys. Acta 625, 248–254. https://doi.org/10.1016/0005-2795(80)90288-3.
Eilaghi, A., Flanagan, J.G., Tertinegg, I., Simmons, C.A., Wayne Brodland, G., Ross Ethier, C., 2010. Biaxial mechanical testing of human sclera. J. Biomech. 43, 1696–1701. https://doi.org/10.1016/j.jbiomech.2010.02.031.
Fujimoto, J.G., 2003. Optical coherence tomography for ultrahigh resolution in vivo imaging. Nat. Biotechnol. 21, 1361–1367. https://doi.org/10.1038/nbt892.
Goth, W., Lesicko, J., Sacks, M.S., Tunnell, J.W., 2016. Optical-based analysis of soft tissue structures. Annu. Rev. Biomed. Eng. 18, 357–385. https://doi.org/10.1146/annurev-bioeng-071114-040625.
Helmchen, F., Denk, W., 2005. Deep tissue two-photon microscopy. Nat. Methods 2, 932–940. https://doi.org/10.1038/nmeth818.
Liao, J., Yang, L., Grashow, J., Sacks, M.S., 2007. The relation between collagen fibril kinematics and mechanical properties in the mitral valve anterior leaflet. J. Biomech. Eng. 129, 78–87. https://doi.org/10.1115/1.2401186.
Masic, A., Bertinetti, L., Schuetz, R., Chang, S.-W., Metzger, T.H., Buehler, M.J., Fratzl, P., 2015. Osmotic pressure induced tensile forces in tendon collagen. Nat. Commun. 6, 5942. https://doi.org/10.1038/ncomms6942.
Meador, W.D., Mathur, M., Sugerman, G.P., Jazwiec, T., Malinowski, M., Bersi, M.R., Timek, T.A., Rausch, M.K., 2020a. A detailed mechanical and microstructural analysis of ovine tricuspid valve leaflets. Acta Biomater. 102, 100–113. https://doi.org/10.1016/j.actbio.2019.11.039.
Meador, W.D., Sugerman, G.P., Story, H.M., Seifert, A.W., Bersi, M.R., Tepole, A.B., Rausch, M.K., 2020b. The regional-dependent biaxial behavior of young and aged mouse skin: a detailed histomechanical characterization, residual strain analysis, and constitutive model. Acta Biomater. 101, 403–413. https://doi.org/10.1016/j.actbio.2019.10.020.
Neu, C.P., Novak, T., Gilliland, K.F., Marshall, P., Calve, S., 2015. Optical clearing in collagen- and proteoglycan-rich osteochondral tissues. Osteoarthr. Cartil.
Rausch, M.K., Bothe, W., Kvitting, J.P.E., Göktepe, S., Craig Miller, D., Kuhl, E., 2011. In vivo dynamic strains of the ovine anterior mitral valve leaflet. J. Biomech. 44, 1149–1157. https://doi.org/10.1016/j.jbiomech.2011.01.020.
Richardson, D.S., Lichtman, J.W., 2015. Clarifying tissue clearing. Cell 162, 246–257. https://doi.org/10.1016/j.cell.2015.06.067.
Rylander, C.G., Stumpp, O.F., Milner, T.E., Kemp, N.J., Mendenhall, J.M., Diller, K.R., Welch, A.J., 2006. Dehydration mechanism of optical clearing in tissue. J. Biomed. Opt. 11,. https://doi.org/10.1117/1.2343208 041117.
Sacks, M.S., 2000. Biaxial mechanical evaluation of planar biological materials. J. Elast. 61, 199–246. https://doi.org/10.1023/A:1010917028671.

Sacks, M.S., David Merryman, W., Schmidt, D.E., 2009. On the biomechanics of heart valve function. J. Biomech. 42, 1804–1824. https://doi.org/10.1016/j.jbiomech.2009.05.015.

Schenke-Layland, K., 2008. Non-invasive multiphoton imaging of extracellular matrix structures. J. Biophotonics 1, 451–462. https://doi.org/10.1002/jbio.200810045.

So, P.T.C., Dong, C.Y., Masters, B.R., Berland, K.M., 2000. Two-photon excitation fluorescence microscopy. Annu. Rev. Biomed. Eng. 2, 399–429. https://doi.org/10.1146/annurev.bioeng.2.1.399.

Stella, J.A., Liao, J., Sacks, M.S., 2007. Time-dependent biaxial mechanical behavior of the aortic heart valve leaflet. J. Biomech. 40, 3169–3177. https://doi.org/10.1016/j.jbiomech.2007.04.001.

Tuchin, V.V., 2005. Optical clearing of tissues and blood using the immersion method. J. Phys. D. Appl. Phys. 38, 2497–2518. https://doi.org/10.1088/0022-3727/38/15/001.

Tuchin, V.V., 1997. Light propagation in tissues with controlled optical properties. J. Biomed. Opt. 2, 401. https://doi.org/10.1117/12.281502.

Xu, X., Wang, R.K., 2004. Synergistic effect of hyperosmotic agents of dimethyl sulfoxide and glycerol on optical clearing of gastric tissue studied with near infrared spectroscopy. Phys. Med. Biol. 49, 457–468. https://doi.org/10.1088/0031-9155/49/3/008.

Xu, X., Zhu, Q., Sun, C., 2009. Assessment of the effects of ultrasound-mediated alcohols on skin optical clearing. J. Biomed. Opt. 14,. https://doi.org/10.1117/1.3156827 034042.

Yeh, A.T., Choi, B., Nelson, J.S., Tromberg, B.J., 2003. Reversible dissociation of collagen in tissues. J. Invest. Dermatol. 121, 1332–1335. https://doi.org/10.1046/j.1523-1747.2003.12634.x.

Zhu, D., Larin, K.V., Luo, Q., Tuchin, V.V., 2013. Recent progress in tissue optical clearing. Laser Photon. Rev. 7, 732–757. https://doi.org/10.1002/lpor.201200056.